The Astrophysical Journal, 646: L77–L80, 2006 July 20

IMAGES OF THE VEGA DUST RING AT 350 AND 450 μm: NEW CLUES TO THE TRAPPING OF MULTIPLE-SIZED DUST PARTICLES IN PLANETARY RESONANCES

K. A. Marsh,[1] C. D. Dowell,[1] T. Velusamy,[1] K. Grogan,[1] and C. A. Beichman[2]

Received 2006 March 6; accepted 2006 June 7; published 2006 July 12

ABSTRACT

We have used the SHARC II camera at Caltech Submillimeter Observatory to make 350 and 450 μm images of the Vega dust disk at spatial resolutions (FWHM) of 9.″7 and 11.″1, respectively. The images show a ringlike morphology (radius ~100 AU) with inhomogeneous structure that is qualitatively different from that previously reported at 850 μm and longer wavelengths. We attribute the 350/450 μm emission to a grain population whose characteristic size (~1 mm) is intermediate between that of the centimeter-sized grains responsible for emission longward of 850 μm and the much smaller grains ($\lesssim$18 μm) in the extensive halo, visible at 70 μm, discussed by Su et al. We have combined our submillimeter images with *Spitzer* data at 70 μm to produce two-dimensional maps of line-of-sight optical depth (relative column density). These "tau maps" suggest that the millimeter-sized grains are located preferentially in three symmetrically located concentrations. If so, then this structure could be understood in terms of the Wyatt model in which planetesimals are trapped in the mean motion resonances of a Neptune-mass planet at 65 AU, provided allowance is made for the spatial distribution of dust grains to differ from that of the parent planetesimals. The peaks of the tau maps are, in fact, located near the expected positions corresponding to the 4 : 3 resonance. If this identification is confirmed by future observations, it would resolve an ambiguity with regard to the location of the planet.

Subject headings: circumstellar matter — planetary systems — stars: individual (Vega)

1. INTRODUCTION

The observable behavior of circumstellar dust particles under the influence of gravity and radiation pressure can provide information on the locations and masses of unseen planets (see, e.g., Wyatt 2003, 2006; Deller & Maddison 2005). A particularly suitable object for study is the A0 star Vega at 7.76 pc, whose disk is seen nearly face-on, as suggested by the low inclination (5°) of the stellar rotation axis (Gulliver et al. 1994). Images at 850 μm and 1.3 mm (Holland et al. 1998; Wilner et al. 2002; Koerner et al. 2001) indicate a partial dust ring ($r \sim 100$ AU) dominated by two unequal clumps interpreted as collisional debris from resonantly trapped planetesimals. More recent observations with the Multiband Imaging Photometer for *Spitzer* (MIPS; Su et al. 2005) have revealed an extensive halo representing small (~2 μm) and medium-sized (~18 μm) grains blown out from the ring by radiation pressure, the ring itself being dominated by large grains of radii $a > 180$ μm.

Dynamical modeling shows the spatial distribution of the ring to be consistent with the 2 : 1(u) resonance of a Neptune-mass planet that has undergone migration (Wyatt 2003). Such a model predicts the existence of other populated resonances (for example 3 : 2 and 4 : 3), the detection of which would help confirm the model and provide new constraints. We present new observations at 350 and 450 μm that bear on this issue.

2. OBSERVATIONS AND DATA REDUCTION

Vega was observed at 350 and 450 μm with the SHARC II camera (Dowell et al. 2003) at the Nasmyth focus of the Caltech Submillimeter Observatory (CSO) on UT 2004 September 17–19 (350 μm; $\tau_{225\,\mathrm{GHz}} \simeq 0.041$), 2005 April 23 (350 μm; $\tau_{225\,\mathrm{GHz}} \simeq 0.036$), and 2005 June 11–13 (450 μm; $\tau_{225\,\mathrm{GHz}} \simeq 0.048$), where $\tau_{225\,\mathrm{GHz}}$ represents the zenith value of atmospheric optical depth. The on-source total integration times were 5.0, 2.7, and 9.7 hr, respectively. Similarly to our Fomalhaut observations (Marsh et al. 2005), the telescope was scanned in an oscillatory fashion in azimuth and elevation with peak-to-peak amplitudes of 30″–100″. The Vega images were generated with an iterative code (SHARCSolve) similar to CRUSH.[3] To reduce spatial $1/f$ noise in the center of the image, the sky intensity was forced to be zero beyond 35″ from the star (analogous to spatial chopping with amplitude 70″ in all directions), except for the final iteration, which allowed nonzero intensities outside 35″ radius for noise-evaluation purposes. After the application of Gaussian smoothing (with a kernel of 5.″5 FWHM), the angular resolutions (FWHM) of the output images were 9.″7 and 11.″1 at 350 and 450 μm, respectively. Absolute calibration was accomplished with hourly, interspersed observations of point sources and is based on assumed Neptune fluxes of $S_{350} = 92.2$ and 86.5 Jy in 2004 and 2005, respectively, and $S_{450} = 65$ Jy. We estimate 1 σ calibration accuracies of 30% and 1″ in absolute flux and pointing, respectively. The flux error includes the effect of subtraction of the slowly varying background (~5% level over spatial scales of a few tens of arcseconds at both wavelengths).

The point-source response function (PSF) was obtained from observations of Mars at 350 μm and Neptune at 450 μm, rotated and co-added to recreate the rotational smearing due to changing parallactic angle. The nonzero angular diameters of those planets (3.″5 and 2.″3, respectively) broadened the estimated PSFs by 6% and 2%, respectively; the effect on subsequent processing was found to be negligible within prevailing errors.

Figure 1 shows the observed images at 350 and 450 μm, before and after subtracting the estimated photospheric contributions of 35 and 21 mJy, respectively. The integrated flux densities of Vega (before photospheric subtraction), within a

[1] Jet Propulsion Laboratory, 4800 Oak Grove Drive, Pasadena, CA 91109; kenneth.a.marsh@jpl.nasa.gov, cdd@submm.caltech.edu, thangasamy.velusamy@jpl.nasa.gov, keith.grogan@jpl.nasa.gov.

[2] California Institute of Technology, IPAC, MS 100-22, Pasadena, CA 91125; chas@ipac.caltech.edu.

[3] See http://www.submm.caltech.edu/~sharc/crush/index.htm.

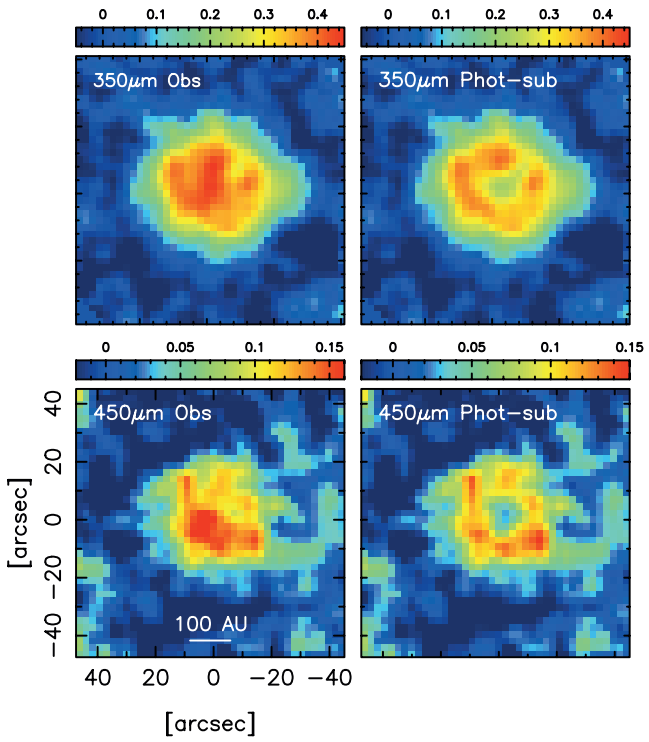

FIG. 1.—Observed and photosphere-subtracted images of Vega at 350 and 450 μm. The intensity scale (shown by the horizontal bar at the top of each image) is in units of mJy arcsec^{-2}, and the orientation is such that north is up and east is to the left. The rms measurement noise on the images is 0.032 and 0.026 mJy arcsec^{-2} at 350 and 450 μm, respectively.

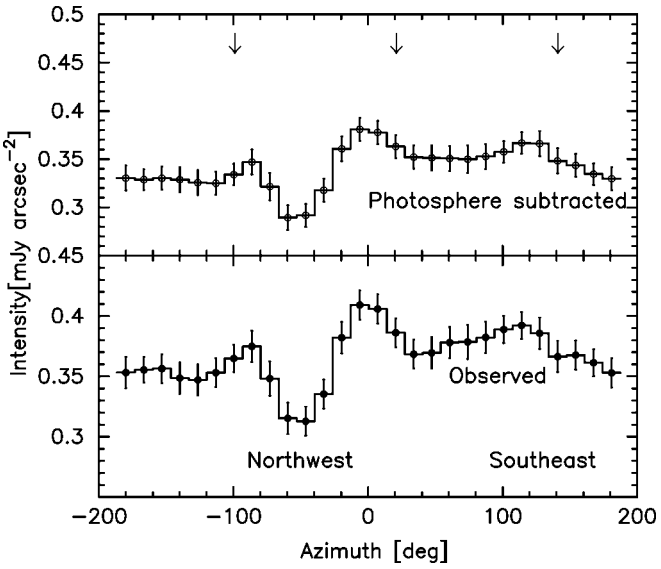

FIG. 2.—Intensity in the Vega disk at 350 μm wavelength as a function of azimuth around the ring (measured east from north), both with and without subtraction of the estimated photospheric contribution. Error bars represent the standard deviation of measurement noise. The arrows represent the expected locations of the 4 : 3 resonance peaks for the dynamical model of Wyatt (2003) in which dust is trapped in the mean motion resonances of a suspected planet.

circular aperture of 30″ radius, at 350 and 450 μm are 500 ± 150 mJy and 150 ± 45 mJy, respectively.

The observed images show clearly the ring morphology of the Vega disk and suggest inhomogeneous structure. Figure 2 shows the 350 μm intensity variation as a function of azimuth, calculated in an annulus of inner and outer radii 6.″9 and 13.″9, respectively. Three peaks are apparent, at azimuths of −90°, 0°, and 120°, with amplitudes of 3, 4, and 2 σ above the local mean level, respectively, where σ represents the statistical measurement noise.

3. MAPPING THE RELATIVE COLUMN DENSITY OF DUST

We have mapped the line-of-sight optical depth (relative column density of dust) in the Vega disk as a function of two-dimensional location in the disk plane using the DISKFIT procedure (Marsh et al. 2005), assuming in this case a geometrically thin face-on disk. The output, referred to as a "tau map," is estimated using a set of observed images at multiple wavelengths, taking full account of the corresponding PSFs. It is assumed that the local temperature of each dust grain component is determined by the energy balance of individual grains in the stellar radiation field using the results of Backman & Paresce (1993). The current version of the code makes simultaneous estimates of the tau maps corresponding to the different grain components, each of which is characterized by the parameters λ_0 and β, where λ_0 represents the wavelength above which the grains radiate inefficiently and which has an approximate correspondence with the grain radius, a, and β is the power-law index of the wavelength dependence of opacity such that $\kappa_\lambda \propto \lambda^{-\beta}$. The spatial resolution of the tau maps exceeds that of the raw images due to implicit deconvolution of the PSFs.

Tau maps were made using data at three wavelengths, by combining our 350 and 450 μm images with a 70 μm MIPS image at the fine (5″) pixel scale. We employed a two-grain model consisting of the 18 μm grains that dominate the 70 μm emission (Su et al. 2005) and a population of larger grains whose size was chosen based primarily on the observed spectral slope between 350 and 70 μm. Specifically, assuming $\beta = 1$ (Dent et al. 2000), the spectral slope implies $T_{\rm dust} \lesssim 50$ K for the larger grains; if we further assume a size-temperature dependence corresponding to the grain composition (silicate-carbon mix) used by Su et al. (2005) in their Vega modeling, we obtain $a \gtrsim 100$ μm. Since this limit was based on the extremes of the flux error bars and of the relative contributions of ring and halo at 70 μm, we have adopted a larger value (1 mm) as being more likely to be representative of the grains responsible for 350/450 μm emission. The results are presented in Figure 3, which shows tau maps for the two grain components (18 μm and 1 mm) separately and also the total optical depth (*bottom panel*). Superposed on the latter, for comparison, are the positions of previously reported emission peaks from longer wavelength data at 850 μm and 1.3 mm (Holland et al. 1998; Koerner et al. 2001; Wilner et al. 2002).

The tau map for 1 mm grains shows inhomogeneities, the reality of which we have assessed using a χ^2 test based on fits to the 350 and 450 μm data. Specifically, an azimuthally uniform ring resulted in a 10% increase in χ^2 relative to an unconstrained tau map; taking into account the number of independent data points (255), this translates into a relative probability of $\sim 5 \times 10^{-6}$, corresponding to a 4.6 σ deviation. We therefore conclude that the azimuthal structure we see in the ring is at the 4–5 σ significance level, consistent with our findings based on the S/N of peaks in the observed 350 μm image (see Fig. 2).

The tau map for 18 μm grains is dominated by a ring of larger scale ($r \simeq 140$ AU) than for the 1 mm grains ($r \simeq$

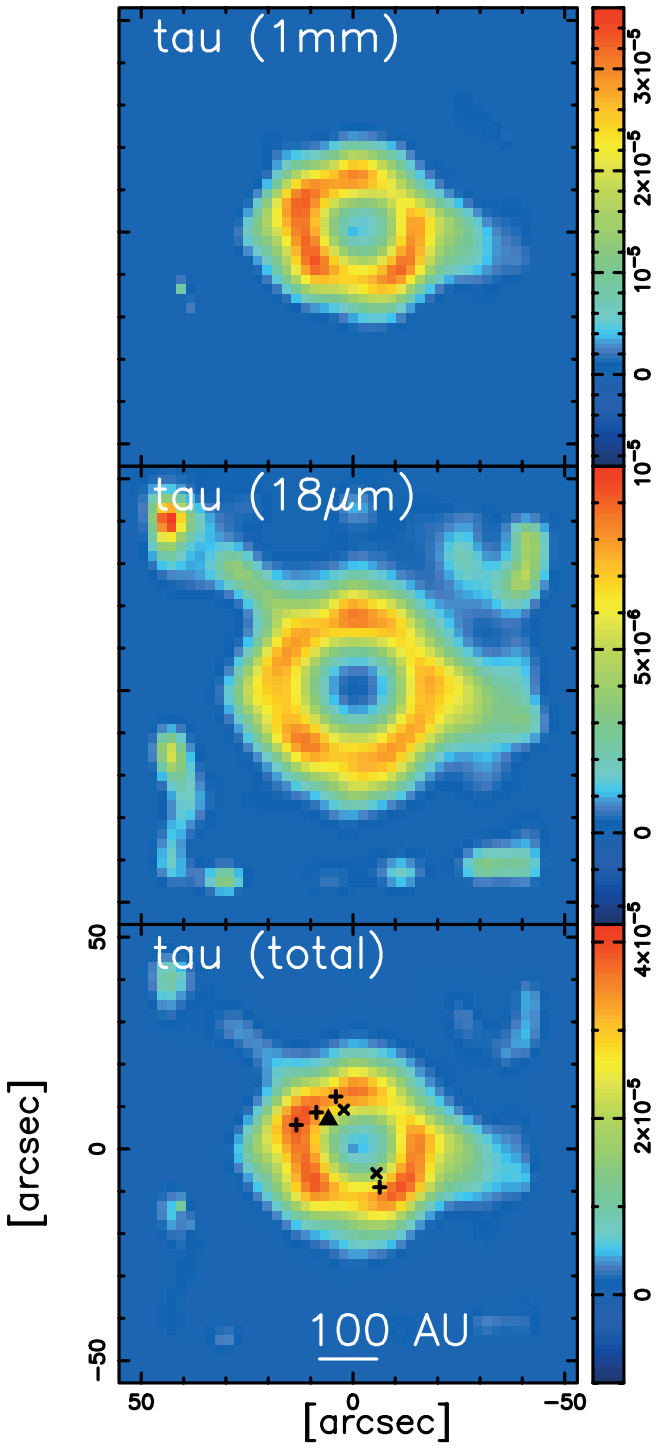

FIG. 3.—Estimated line-of-sight optical depth of the Vega disk at a reference wavelength of 350 μm, based on observed images at 350, 450, and 70 μm, assuming a two-component dust grain model in which the grain radii are 1 mm and 18 μm. The top and middle panels show the optical depth distribution for the two grain components separately, while the bottom panel shows the sum of both components. Also shown on the lower plot are the locations of previously reported emission peaks from longer wavelength data as follows: *filled triangle*, 850 μm (Holland et al. 1998); *crosses*, 1.3 mm (Wilner et al. 2002); *plus signs*, 1.3 mm (Koerner et al. 2001).

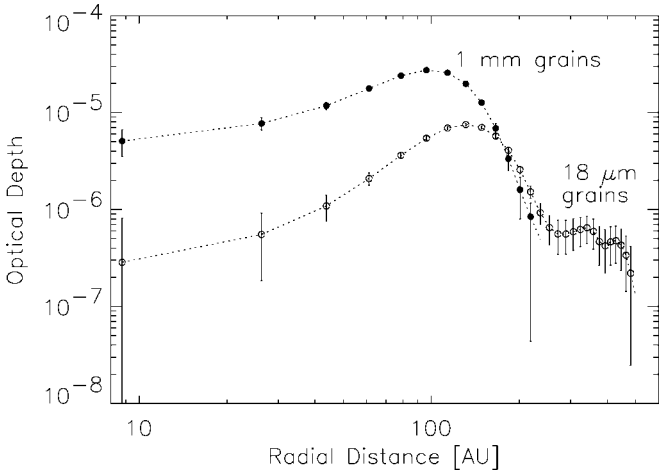

FIG. 4.—Radial profiles of estimated optical depth for the two grain components, characterized by grain radii of 1 mm (*filled circles*) and 18 μm (*open circles*).

100 AU). There is also lower level diffuse structure masked by surrounding noise spikes, the latter resulting from the radial increase in tau estimation error corresponding to decreasing dust temperature. We can, however, smooth out these fluctuations with azimuthal averaging to show the underlying diffuse structure. Figure 4 shows the result in the form of radial profile plots of the 1 mm grain component (*filled circles*) and the 18 μm grain component (*open circles*). The error bars reflect the tau map estimation errors after a $\sqrt{N}$ reduction from azimuthal averaging in annuli of width 17.5 AU. It is apparent that for $r > 200$ AU, the radial falloff in column density of 18 μm grains is consistent with the $1/r$ variation reported by Su et al. (2005). Inside 200 AU, however, some of these grains may be concentrated in the ring structure, but the proportion is subject to model uncertainties related to the larger grain component.

4. INTERPRETATION

The observations show the qualitatively different appearance of the Vega dust ring at 350/450 μm and ≥850 μm. Furthermore, the 850 μm flux (23 mJy) predicted by our tau map accounts for only a fraction of either of the published values of 850 μm flux, which are 45.7 ± 5.4 Jy (Holland et al. 1998) and 91 mJy (W. S. Holland et al., in preparation; as quoted by Su et al. 2005). The observations can, however, be reconciled using a model in which the ring emission at 350/450 μm is dominated by 1 mm grains with a λ^{-1} opacity law, and the emission longward of 850 μm is dominated by an additional component of much larger grains with flat spectral opacity ($\beta \sim 0$); the latter would require grain sizes of at least a centimeter (Pollack et al. 1994).

The morphology of the 850 μm image (with its single dominant peak at ~45° in position angle) has been attributed to dynamical effects, the most important of which is the 2 : 1(u) resonance of a Neptune-mass planet 65 AU from the star (Wyatt 2003). Those calculations also show that other resonances are present, principally 3 : 2 and 4 : 3, the latter of which shows a threefold spatial symmetry consistent with what we see at 350/450 μm. In this regard we note that for a planet of a given mass, the requirement that the dust grains not be dislodged from resonance by radiation pressure sets a lower limit, $a_{\rm crit}$, to the grain size (Wyatt 2006). For a Neptune-mass planet

orbiting Vega (luminosity 60 $L_{\odot}$, mass 2.5 $M_{\odot}$), Wyatt's expression leads to $a_{\rm crit} = 900$ μm, consistent with our choice of $a = 1$ mm for the tau maps.

Based on the 850 μm data alone, an ambiguity exists for the orbital direction of the planet, shown counterclockwise in Figure 15*b* of Wyatt (2003). But if our identification of the 350/450 μm structure with the 4 : 3 resonance is correct, then the ambiguity is resolved; the planet is then located diametrically opposite to the star from the southeastern clump in our Figure 3 and its orbit is clockwise. The predicted locations of the 4 : 3 resonance peaks are then given by the arrows in Figure 2, which are in substantial agreement with observation.

It would then remain to explain why the centimeter-sized grains (seen at 850 μm) and millimeter-sized grains (seen at 350/450 μm) exhibit two different resonance patterns. We note, however, that the analysis by Su et al. (2005) suggests that the dust has been released during a relatively recent event, most likely the collision of two planetesimals. This being the case, our results could be understood if the two planetesimals involved were located in the 4 : 3 resonance, and if the collision released smaller particles than the ones that were there before, thus affecting the 350/450 μm appearance much more than that at 850 μm. The 4 : 3 resonance is, in fact, a relatively likely place for a collision to occur, since the collision timescale decreases with decreasing orbital semimajor axis, and hence is shorter in the 4 : 3 resonance than in 2 : 1.

We have simulated this scenario with dynamical modeling based on a Neptune-mass planet at 65 AU, assuming orbital parameters similar to Wyatt (2003), and further assuming that the 4 : 3 resonance is populated by smaller grains (1 mm) than the other resonances (1 cm). The results are presented in Figure 5. Comparison of the predicted 350 and 850 μm images with the observations (our Fig. 1 and Holland et al. 1998, respectively) shows that the model successfully accounts for the wavelength dependence of the observed structure. Our analysis therefore suggests that different resonances can be populated by grain populations of different sizes, depending on the collisional history of the planetesimals. This means that the dust distribution does not necessarily mimic the planetesimal distribution as assumed by Wyatt (2003). It will thus be important to confirm the detection of the 4 : 3 resonance and constrain the grain sizes involved using future observations at multiple wavelengths.

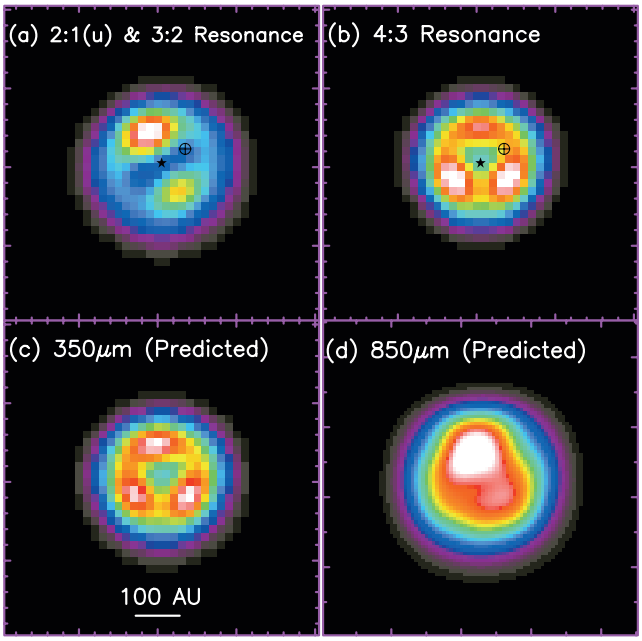

FIG. 5.—Results of dynamical modeling of the Vega dust disk showing the predicted intensity distributions of dust emission at 350 and 850 μm. Following Wyatt (2003) we assume a Neptune-mass planet at 65 AU, and further assume that the planet orbits clockwise, that it is currently located northwest of the star, and that its 4 : 3 resonance is populated by smaller grains (1 mm) than the other resonances (1 cm). *Top panels*: The 350 μm emission resulting from (*a*) the combined effects of the 2 : 1(u) and 3 : 2 resonances, and (*b*) the 4 : 3 resonance. The planet is indicated by an encircled plus sign. *Bottom panels*: Predicted observational images at (*c*) 350 μm and (*d*) 850 μm. Images *c* and *d* were produced by adjusting the relative amounts of material in the two grain populations (1 mm and 1 cm) to provide the best match to the observed images; this required equal amounts of material (by cross-sectional area) in each. In this model, the 1 mm grains (4 : 3 resonance) contribute 80% ± 16% of the observed flux at 350 μm and 60% ± 12% at 850 μm, while the 1 cm grains [2 : 1(u) and 3 : 2 resonances] contribute 20% at 350 μm and 40% at 850 μm. All of the above images have been smoothed to the spatial resolution of the observations, corresponding to FWHMs of 10″ at 350 μm (CSO SHARC II; present paper) and 14″ at 850 μm (JCMT SCUBA; Holland et al. 1998). On the linear pseudocolor intensity scale, white corresponds to peak intensity for each individual image.

This work was performed by the Jet Propulsion Laboratory, California Institute of Technology, under contract with the National Aeronautics and Space Administration. Research at the Caltech Submillimeter Observatory is supported by NSF grant AST 02-29008.

REFERENCES

Backman, D. E., & Paresce, F. 1993, in Protostars and Planets III (Tucson: Univ. Arizona Press), 1253
Deller, A. T., & Maddison, S. T. 2005, ApJ, 625, 398
Dent, W. R. F., Walker, H. J., Holland, W. S., & Greaves, J. S. 2000, MNRAS, 314, 702
Dowell, C. D., et al. 2003, Proc. SPIE, 4855, 73
Gulliver, A. F., Hill, G., & Adelman, S. J. 1994, ApJ, 429, L81
Holland, W. S., et al. 1998, Nature, 392, 788
Koerner, D. W., Sargent, A. I., & Ostroff, N. A. 2001, ApJ, 560, L181
Marsh, K. A., Velusamy, T., Dowell, C. D., Grogan, K., & Beichman, C. A. 2005, ApJ, 620, L47
Pollack, J. B., Hollenbach, D., Beckwith, S., Simonelli, D. P., Roush, T., & Fong, W. 1994, ApJ, 421, 615
Su, K. Y. L., et al. 2005, ApJ, 628, 487
Wilner, D. J., Holman, M. J., Kuchner, M. J., & Ho, P. T. P. 2002, ApJ, 569, L115
Wyatt, M. C. 2003, ApJ, 598, 1321
———. 2006, ApJ, 639, 1153